

Latitudinal Structure of Dayside Polar Cusp Precipitation

V. G. Vorobjev^{a, *}, O. I. Yagodkina^{a, **}, E. E. Antonova^{a, b, ***}, and I. P. Kirpichev^{c, ****}

^a Polar Geophysical Institute, Apatity, Murmansk oblast, Russia

^b Skobel'syn Institute of Nuclear Physics, Moscow State University, Moscow, Russia

^c Space Research Institute, Russian Academy of Sciences, Moscow, Russia

*e-mail: vorobjev@pgia.ru

**e-mail: oksana41@mail.ru

***e-mail: elizaveta.antonova@gmail.com

****e-mail: ikir@iki.rssi.ru

Received April 6, 2023; revised July 6, 2023; accepted August 3, 2023

Abstract—The results of observations of low-altitude spacecraft crossing the daytime sector of the auroral zone and of high-apogee spacecraft in the equatorial plane of the magnetosphere were analyzed in order to identify the main processes leading to the formation of dayside polar cusps. Observations from the DMSP F7 spacecraft were used to analyze the latitudinal characteristics of ion precipitation in the cusp region and to study the latitudinal profile of ion pressure in the cusp depending on the IMF parameters. A significant difference was found in identifying the cusp boundaries using an automated data processing system and direct analysis of spacecraft observations. It is shown that for small negative values of the B_z -component of the IMF ($\langle B_z \rangle = -3.0$ nT), an ordinary feature of the cusp is the latitudinal profile of the ion pressure (P_i) with a width of $\sim 1^\circ$ of latitude with two maxima, one of which is located in the equatorward and the other in the poleward of the cusp. For large negative B_z values ($-6, -8$ nT), the polar maximum in the latitudinal profile P_i disappears; only the equatorial maximum remains, the P_i level at the maximum increases, and the width of the cusp decreases to $\sim 0.7^\circ$. For B_z IMF > 0 , the most characteristic is the P_i profile with a maximum ion pressure in the polar part of the cusp. The cusp for $B_z > 0$ is located at higher latitudes than for $B_z < 0$, and its average latitudinal width increase to $\sim 1.4^\circ$ of latitude. In the prenoon sector MLT, the most typical for periods with a large negative B_y -component of the IMF ($\langle B_y \rangle = -6.3$ nT, $\langle B_z \rangle = -1.7$ nT) is a cusp with a width of $\sim 1.4^\circ$ of latitude with a flat top in the latitudinal P_i profile. Comparison of the pressure distributions observed at low heights with data from high-apogee satellites confirmed the possibility of describing the formation of the cusp as a diamagnetic cavity and using observations in the cusp to determine the ion pressure in the magnetosheath.

DOI: 10.1134/S0016793223600662

1. INTRODUCTION

Polar cusps (one in each hemisphere) arise as a result of the solar wind plasma flowing around the geomagnetic dipole and distortion of the dipole field by currents flowing in the magnetosphere. Each polar cusp is a diamagnetic funnel-shaped structure (Pitout and Bogdanova, 2021). The plasma of the magnetosheath in the cusp regions penetrates to ionospheric heights and is recorded by low-altitude auroral satellites. With increasing dynamic solar wind pressure (P_{sw}), the longitudinal and latitudinal dimensions of the cusp increase, as well as the energy fluxes of magnetosheath particles precipitating in the region of the polar cusp (Newell and Meng, 1994; Vorobjov and Yagodkina, 2022).

At ionospheric heights, the cusp is usually observed at corrected geomagnetic latitudes from 74° to 78° CGL depending mainly on the dipole tilt angle, the level of geomagnetic activity, and the B_z -

and B_y -components of the interplanetary magnetic field (IMF). Large-scale characteristics of the cusp were obtained several decades ago from observations of precipitating particles by low-altitude polar-orbiting satellites of the DMSP series. According to statistical studies (Newell and Meng, 1988; Newell et al., 1989, 1991; etc.), the cusp at the heights of the DMSP satellite is a region with dimensions of $\sim 1^\circ$ of latitude and ~ 2.5 h MLT in longitude. The cusp is approximately symmetrical relative to its central part, usually located in the area of the noon meridian, and shifts in the Northern Hemisphere by ~ 1 h MLT in the prenoon (afternoon) direction with negative (positive) values of the B_y -component. At a very high level of the dynamic solar wind pressure ($P_{sw} \sim 20$ nPa), the width of the cusp can be 2.0° – 2.5° of latitude (Vorobjev and Yagodkina, 2022), and already for $P_{sw} \sim 6$ nPa, the average longitudinal dimensions of the cusp increase to 4.8 h MLT (Newell and Meng, 1994).

The cusp is very dynamic; its characteristics change rapidly following changes in the external impact parameters. Observations by CLUSTER project satellites at middle heights in the cusp indicate a very rapid response of the cusp to changes in the IMF: currents in the cusp begin to change already within $\sim 1\text{--}2$ min after a change in the IMF (Pitout and Bogdanova, 2021). The solar wind has a high level of turbulent fluctuations with complex nonlinear relationships between fluctuating parameters. Therefore, separating the influence of each parameter by the characteristics of polar cusp precipitation is an extremely difficult problem. Despite numerous studies published in the last two to three decades, the influence of individual parameters of the solar wind plasma and IMF on the structure of polar cusp precipitation and even their large-scale characteristics remain completely unexplored. Thus, in (Wing et al., 2001), based on an analysis of DMSP satellite observations for 1985–1995, it was concluded that the latitudinal dimensions of the cusp increase with increasing absolute values of both the B_z - and B_y -components. However, on the one hand, significant IMF components are often accompanied by high P_{sw} levels. On the other hand, the scatter of data in this study is so large and the correlation coefficients so low that we can only speak about some tendency towards an increase in the latitudinal dimensions of the cusp. It was found that when $|B_z|$ and $|B_y| < 5$ nT, the latitudinal dimensions of the cusp are only $\sim 0.5^\circ\text{--}0.7^\circ$ of latitude and increase on average to $\sim 1^\circ$ for $|B_z|$ or $|B_y| > 5$ nT. In contrast to this statement, the authors of the review article (Pitout and Bogdanova, 2021) point out that for large values of the negative B_z -component, the cusp can be very narrow in terms of latitude. Thus, in (Bogdanova et al., 2007), the results of the cusp recorded by CLUSTER satellites were analyzed. At extremely high values of the southern component of the IMF, a cusp width of less than 1° was recorded, while under average normal conditions, the width of the cusp at the height of the CLUSTER satellites is $> 2^\circ$. Note that the MHD simulation carried out in (Siscoe et al., 2007) shows good agreement with these observation results.

Studies on simulating cusp formation mainly analyze regular, relatively fast plasma flows and movements of particle groups in regular fields. The penetration of magnetosheath particles into the magnetosphere and the formation in the area of the dayside magnetopause of such structures as the low-latitude boundary layer, cusp, and plasma mantle have been modeled (Onsager et al., 1993; Wing et al., 1996; Wing et al., 2001; etc.). For example, in (Wing et al., 2001), a model of particle precipitation on open field lines is presented using an empirical electric field model obtained statistically from long-term radar observations at the Goose Bay Observatory. For small values of the southern IMF component and in the presence of a strong azimuthal component, the model described the occurrence of a double cusp. In the mid-

day sector, one cusp was located at lower, and the other at higher latitudes. The high-latitude cusp appeared in a region of strong azimuthal and poleward convection, due to which a polar-orbiting satellite should record the latitudinal dispersion of the energy of precipitating particles. The cusp at a lower latitude was located in a region of weak azimuthal convection and was therefore considered dispersion-free. The study (Wing et al., 2001) also presents individual flybys of DMSP satellites, which, from the authors' viewpoint, confirm the prediction of the model. The case of recording of a double cusp from CLUSTER satellite observations is also discussed in (Escoubet et al., 2008). A statistical study of cusp morphology based on observations from CLUSTER satellites was carried out in (Pitout et al., 2009). As the authors of the cited study indicate, out of 261 cusp observations for 2001–2004, only 12 can be attributed to the recording of a double cusp with a relatively stable IMF. In ten of these events, a double cusp was observed with a northward orientation of the B_z -component. The observation of two cusp sources, one at lower and the other at higher latitudes, is described in (Fuselier et al., 2000) based on observations from the Polar satellite for a northern IMF and a high level of the solar wind dynamic pressure (P_{sw}). Signs of two maxima in ion precipitation of the cusp for the northern IMF and high P_{sw} values were also discovered in (Vorobjev and Yagodkina, 2022) based on DMSP satellite data. Meanwhile, the MHD modeling of the cusp at the northern IMF carried out in (Esmaili and Kalaei, 2017) does not show a clearly expressed double maximum in the ion population, however the possibility of rapid changes of the localization and large-scale cusp characteristics under conditions of sharp changes of the solar wind parameters and the IMF makes the assumption of the contribution of a temporary effect probable.

The dynamics of the precipitation at auroral latitudes, recorded by low-flying satellites, during modeling is governed by the dynamics of the magnetospheric magnetic field and the distribution of large-scale electric fields (magnetospheric convection pattern). The observed patterns are usually described by models of a closed and open magnetosphere and the idea of the dominant role of reconnection processes (see, e.g., (Reiff et al., 1977; Sonnerup et al., 1981) and numerous later works). However, such ideas encounter certain difficulties in areas where the plasma speeds are much lower than the sonic and Alfvén speeds and the condition of magnetostatic equilibrium is satisfied (Antonova and Stepanova, 2021; Antonova et al., 2023). The magnetopause was initially defined as a current layer across which balance of the plasma pressure and magnetic field of the magnetosheath and magnetosphere occurs. Such a layer is not easy to identify in the outer part of the cusp, where the magnetic field is weak and a high level of turbulent fluctuations is constantly observed. However, Panov et al.

(2008) successfully demonstrated the existence, on average, of pressure balance between the plasma of the magnetosheath and the cusp, using observational data from the CLUSTER project. This balance means that it is possible to use the results of fluctuation-averaged measurements of low-flying satellites crossing the cusp precipitation region to determine the total pressure in the magnetosheath in front of the cusp, since under conditions of magnetostatic equilibrium, the plasma pressure is constant along the magnetic field line. The magnitude of the plasma pressure in the cusp determines the magnitude of depression of the magnetic field in the cusp region and, consequently, the distortion of the magnetic field. However, despite the fact that analysis of pressures by auroral satellites and in the equatorial plane made it possible to clarify the problem of projecting an auroral oval onto the equatorial plane of the magnetosphere using the morphological projection method (Antonova et al., 2014; Antonova et al., 2015, 2018), studies of pressure distribution when auroral satellites cross the cusp region have only just begun (Vorobjev et al., 2020). Averaged pressure values and their dependences on the solar wind dynamic pressure and the B_z -component of the IMF were obtained. Such studies can serve as a basis for creating alternative cusp formation models that analyze the pressure balance. Such studies, first of all, require verification of previously obtained experimental patterns and analysis of pressure distribution obtained from data of low-flying satellites in the cusp precipitation region.

The aim of this study is to determine the morphological characteristics of ion precipitation in the dayside polar cusp and ion pressure in the cusp and to study the features of the latitudinal distribution of energy fluxes of precipitating ions and their relationship with the B_z - and B_y -components of the IMF. Particular attention is paid to determining the latitudinal position of the equatorward and poleward boundaries of the cusp and determining the state of the IMF during their recording periods. The results of pressure distribution analysis by low-flying satellites are compared with the average pressure distribution in the magnetosheath near the equatorial plane.

2. DATA USED

The study used data from the DMSP F7 satellite for all of 1986. This was a year of a quiet Sun at the very beginning of the 22nd solar activity cycle. The satellite had an almost circular polar orbit at an height of ~ 835 km and an orbital period of ~ 101 min. Every second, the satellite recorded the spectrum of precipitating particles in the energy range from 32 eV to 30 keV in 19 channels distributed over energies in a logarithmic sequence. In 1 s, the satellite moves a distance of ~ 7.5 km, which, taking into account the deviation of its trajectory from the geomagnetic meridian, on average corresponds to $\sim 0.05^\circ$ CGL. It should be noted

that the orbits of the F7 satellite provided optimal opportunities for observing cusp precipitation, which was, as a rule, difficult during subsequent implementation of the DMSP program.

To select flybys of the F7 satellite during which the dayside polar cusp was recorded, we used data from an automated processing system (APS), the operating principle of which was published in (Newell et al., 1991). The positions of the equatorward and poleward boundaries of the cusp were taken both from the APS tables and were obtained by the authors themselves from an analysis of the initial satellite data. F7 satellite data and APS tables are presented at <http://civspace.jhuapl.edu>. The satellite's corrected geomagnetic coordinates (Φ' and MLT) projected along field lines to an height of 110 km were determined using the AACGM model (Baker and Wing, 1989). Data during periods of magnetic storms ($Dst < -15$ nT) were not considered.

The pressure created by fluxes of precipitating ions significantly exceeds the electron pressure, which is less than 15% of the total plasma pressure. The methodology for determining ion pressure from DMSP satellite measurements was published in (Wing and Newell, 1998). In this study, we use a modified version of this technique proposed in (Stepanova et al., 2006). The ion pressure is calculated under the assumption of a Maxwellian energy distribution of particles; i.e., this study did not take into account the contribution of energetic particles to the total pressure, which does not make significant corrections when considering the spectra of particles penetrating from the magnetosheath (Kirpichev et al., 2017).

Data about the solar wind plasma and IMF parameters were taken from the OMNIWeb portal (<http://cdaweb.gsfc.nasa.gov/>). As noted above, the characteristics of the plasma in the cusp region begin to change within 1–2 min after a change in the external influence conditions. The cusp is very variable, but also quite inertial: approximately 20 min are required to establish full correspondence of the latitudinal position and size of the cusp in response to changes in external conditions (Pitout and Bogdanova, 2021). Therefore, to study the influence of the IMF components on the precipitation characteristics, we used the average values of the parameters of the interplanetary medium observed over 20 min prior to recording of the cusp by the F7 satellite. In our study, hourly average IMF values could not be used, which significantly affected the statistics of these events: first, because the hourly average values of the IMF components often differ radically both in magnitude and direction from what is observed immediately before the recording of the cusp; second, when hourly averages are available, data on the IMF immediately before recording of the cusp are often missing, at least in 1986.

Using the values of IMF components exclusively during the period of cusp recording for the study,

which for the F7 satellite is usually 1–2 min, can also lead to erroneous conclusions due to some inertia of cusp precipitation. It is also necessary to take into account the high level of fluctuations of the magnetic field and plasma parameters after the solar wind passes a bow-shock (see, e.g., the review (Rakhmanova et al., 2021)). In this case, the magnetic field immediately before the magnetopause can differ radically, even in sign, from the direction of the magnetic field in the solar wind (Pulinetz et al., 2012).

3. DETERMINATION OF THE EQUATORWARD AND POLEWARD BOUNDARIES OF THE CUSP

3.1. Analysis of F7 Satellite Data

By comparing satellite observations at different heights, Newell and Meng (1988) obtained the typical characteristics of particles in different precipitation regions of the dayside sector and determined the criteria making it possible to identify precipitation in the cusp and adjacent areas based on low-altitude satellite observations of precipitating particles. Newell et al. (1991) present an automated processing system (APS) of satellite information, which determines the structure of auroral precipitation based on data from DMSP series satellites. The APS is based on an artificial neural network with one hidden layer, trained on a number of examples, allowing correction of identification errors. Data on the structure of precipitation in each flyby are presented in tables showing, among other things, the corrected geomagnetic coordinates of the boundaries of various types of precipitation. Polar cusp precipitation is identified when the following criteria, formulated in (Newell and Meng, 1988), are simultaneously met:

— average energy: ions $300 \text{ eV} < Ei < 3000 \text{ eV}$, electrons $Ee < 220 \text{ eV}$;

— energy flux: ions $Fi > 10^{10} \text{ eV/cm}^2 \text{ s sr}$, electrons $Fe > 6 \times 10^{10} \text{ eV/cm}^2 \text{ s sr}$.

In this work, APS data were used to select flybys of the F7 satellite in which cusp precipitation was identified. In total, 798 such flybys were recorded in 1986, which is 14% of the total number of satellite flybys in the dayside sector. In the narrower sector of 1000–1400 MLT, 543 cases of cusp recording were found. From these events, satellite flybys with a recorded classical sequence of dayside precipitation regions with increasing of the latitude were selected: low-latitude boundary layer (*LLBL*)–cusp–mantle. Recording of areas adjacent to the cusp is a guarantee that the satellite completely crossed the cusp, from its equatorial boundary to the polar. Only areas recorded by the satellite for more than four times since the flight time were considered. A total of 142 cusp crossings were detected over the 1-year observation period for which solar wind plasma and IMF data were available.

Since one of the main goals here was to study the latitudinal characteristics of ion precipitation in the cusp region, for most of the selected flybys, the initial F7 satellite data were analyzing, including determining the latitude of its equatorial and polar boundaries. To determine the cusp boundaries, the same criteria were used as for automated data processing. In most cases, the latitudinal position of the cusp boundaries obtained from such an analysis does not coincide with published the APS data. One such example is shown in Fig. 1: the characteristics of precipitating particles in the dayside sector on June 28, 1986, in the interval rounded 0129–0131 UT. The polar cusp in this flyby was recorded in the Southern Hemisphere at approximately 0130 UT at a longitude of ~ 11.9 MLT. Figure 1a shows fluxes of precipitating ions and electrons (Fi , Fe) in units of $\text{eV/cm}^2 \text{ s sr}$; Fig. 1b shows their average energies (Ei , Ee , keV). The points on the graphs correspond to the values of the parameters measured by the satellite. The horizontal axis represents the corrected geomagnetic latitude (CGL). The cusp boundaries were determined in accordance with the above-mentioned criteria, the level of which for all categories of parameters is shown by horizontal dashed lines, and the boundaries of the cusp, by vertical dashed lines. The equatorial boundary of the cusp in this flyby is determined by the average energy of ion precipitation (Ei), and the polar boundary, by the energy flux of electron precipitation (Fe). In this case, as in the APS, the sequence of identifications cusp–cusp–not cusp–cusp–cusp was defined as the cusp.

Figure 2a shows the latitudinal distribution of the energy flux of precipitating ions, but in units of $\text{erg/cm}^2 \text{ s}$. Vertical dashed lines show the cusp boundaries defined in Fig. 1 from the analysis of satellite data, and the solid vertical lines are the cusp boundaries determined by the APS. Clearly, there is a significant, approximately 0.3° CGL, discrepancy in the position of the boundaries. Moreover, in this F7 flyby, the width of the cusp ($\Delta\Phi'$), determined from the difference of latitudes of its polar and equatorial boundaries, in Fig. 1 and according to the APS tables are approximately the same. However, in other satellite flybys, the discrepancy in the position of the boundaries is followed by discrepancies in the latitudinal dimensions of the cusp. Of the 142 flybys selected according to APS data in the “manual” analysis mode, 106 flybys were considered.

The probability of the cusp observation with a different latitudinal extent is shown in Fig. 3. Figure 3a shows the distribution obtained from APS data; the total number of events $N = 142$. The horizontal axis shows the width of the cusp in degrees of CGL. The vertical axis is the number of cusp recordings normalized to the maximum in each range $\Delta\Phi'$ at 0.1° . The average cusp width $\Delta\Phi'_c = 0.6^\circ$; the median cusp width $\Delta\Phi'_m = 0.5^\circ$. Figure 3b shows a similar distribution, but which was obtained as a result of direct detailed

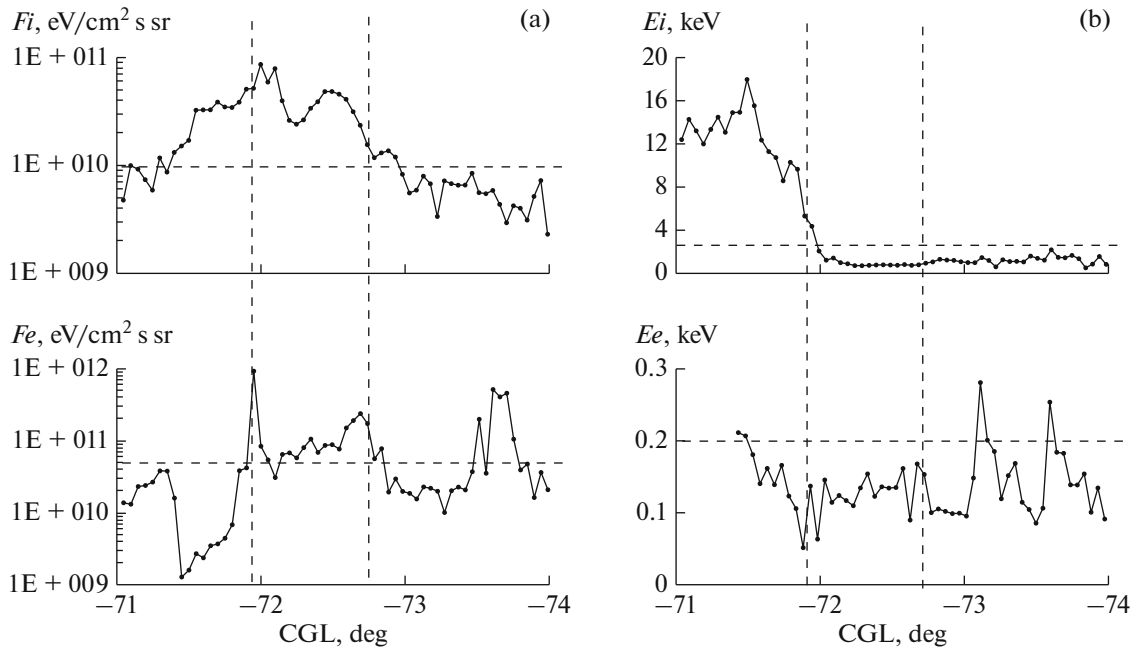


Fig. 1. Fluxes of energy (F_i , F_e) and average energies (E_i , E_e) of precipitating ions and electrons in midday sector, recorded by F7 satellite on June 28, 1986, in interval 0129–0131 UT. Horizontal dashed lines, level of criteria for determining cusp; vertical dashed lines, cusp boundaries.

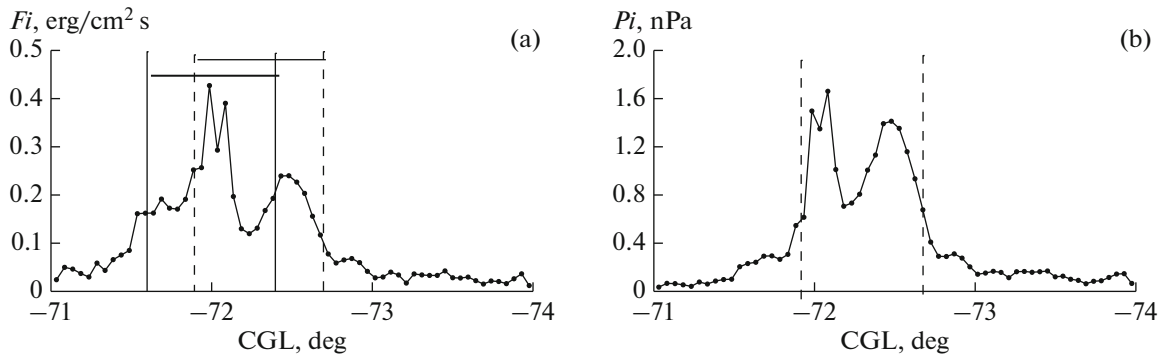


Fig. 2. Latitudinal distribution of energy flux of precipitating ions (a) and ion pressure (b) in dayside sector on June 28, 1986, in interval 0129–0131 UT. Vertical dashed lines, cusp boundaries determined from analysis of satellite data; solid vertical lines, cusp boundaries determined by APS.

analysis of satellite observations. For this distribution ($N = 106$), the average cusp width $\Delta\Phi'_c = 1.0^\circ$, and the median cusp width $\Delta\Phi'_m = 0.9^\circ$. Such a significant difference in the cusp width, $\sim 0.3^\circ$ of latitude, is due to the difference in identification of the cusp boundaries by APS and direct analysis of satellite observations. As Fig. 3b shows, $\Delta\Phi'$ can reach $\sim 3.0^\circ$ of latitude, but the cusp can also be very narrow, $\sim 0.2^\circ$.

3.2. Position and Width of the Cusp Depending on the B_z - and B_y - Components of the IMF

In further studies, we use data on the position of the cusp boundaries obtained from direct analysis of satellite observations. As a test, in Fig. 4a, the depen-

dence of the latitudinal position of the equatorial boundary of the cusp on the B_z -component is studied. It is well known (Wing et al., 2001; Pitout and Bogdanova, 2021 and references therein), that with the southern orientation of the IMF, the equatorial boundary of the cusp (Φ'_{eq}) shifts toward the equator with a decrease in the B_z -component. With a northern orientation of the IMF, the position of the equatorial boundary of the cusp does not depend or weakly depends on the value of the positive B_z . Solid lines in Fig. 4a correspond to linear regression equations individually for $B_z < 0$ and $B_z > 0$. The regression equations are $\Phi'_{eq} = 77.9 + 0.73B_z$ (correlation coefficient $r_1 = 0.70$) and $\Phi'_{eq} = 77.8 + 0.01B_z$ (correlation coef-

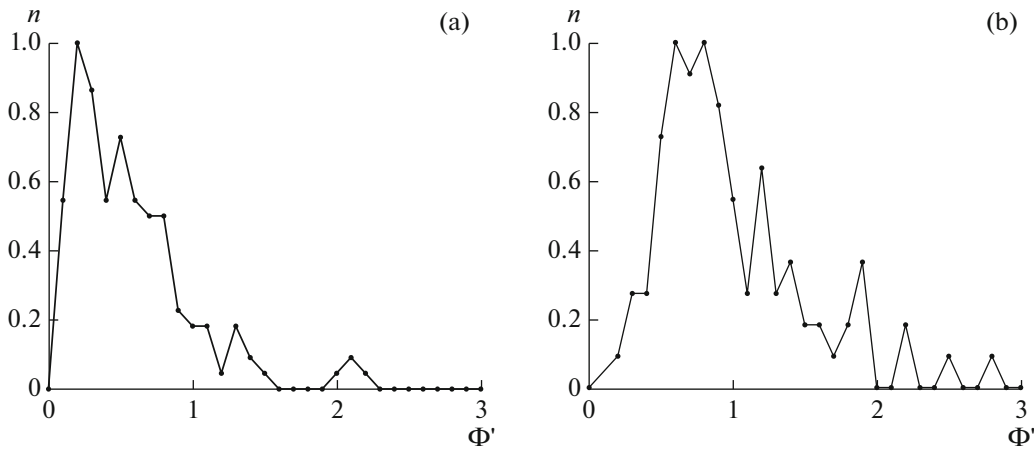


Fig. 3. Observations of cusp with various latitudinal extents: (a) distribution obtained from APS data, (b) distribution obtained from direct analysis of satellite observations. Horizontal axis, cusp width in degrees CGL; vertical axis, number of cusp recordings normalized to maximum in each range $\Delta\Phi'$ by 0.1° .

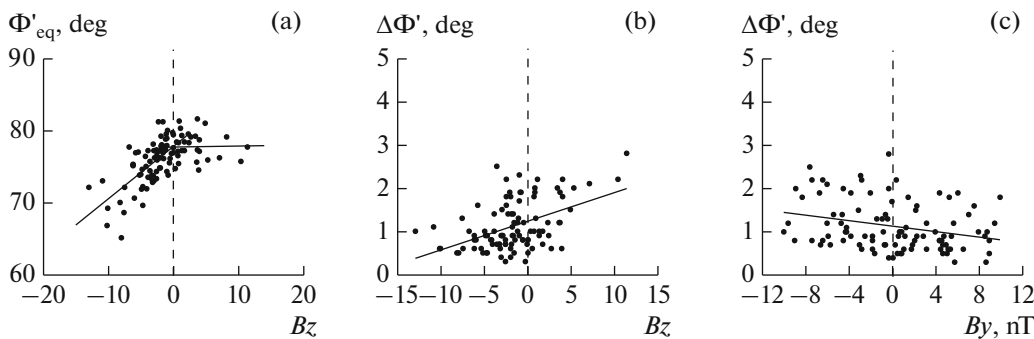


Fig. 4. (a) Latitude of equatorial boundary of cusp depending on B_z -component of IMF; dependence of latitudinal width of cusp on (b) B_z - and (c) B_y -components of IMF. Solid lines correspond to linear regression equations.

ficient $r_2 = 0.22$) for $B_z < 0$ and $B_z > 0$ accordingly. The nature of the behavior $\Phi'_{eq} = \Phi'(B_z)$ is similar to that obtained by other researchers. Regression equations best fit the data (Wing et al., 2001); however, the correlation coefficient for our dataset is significantly higher than 0.54 and 0.04 for $B_z < 0$ and $B_z > 0$, respectively, in (Wing et al., 2001).

Figures 4b and 4c show the dependence of the latitudinal width of the cusp from the B_z - and B_y -components. Solid lines in the figures correspond to linear regression equations with correlation coefficients $r = 0.47$ and $r = 0.25$ for the B_z - and B_y -components, respectively. The scatter of $\Delta\Phi'$ values is significant in the plots, which may be covered by the influence on the cusp width of other IMF components and parameters such as P_{sw} , dipole tilt angle, MLT of cusp recording, etc. However, Fig. 4b reliably indicates the following two factors: the first, on average, the cusp is much wider for $B_z > 0$ than for $B_z < 0$, and the second, on average, $\Delta\Phi'$ decreases with decreasing B_z .

Figure 4c shows $\Delta\Phi'$ as a function of the B_y -component. The scatter of points on the plot with respect

to the linear regression equation is $\sim 1^\circ$ or more. Despite the low correlation coefficient, a small but systematic decrease in $\Delta\Phi'$ can be seen with an increase in B_y . Such behavior of $\Delta\Phi'$ may be due to different cusp width depending on the MLT of its recording. Vorobjev and Yagodkina (2022) considers an event when, for $B_y < 0$, the cusp is significantly wider in the prenoon sector than in the afternoon sector. The average longitude of the satellite crossing the area of dayside precipitation over the entire dataset used in Fig. 4 is 11.3 MLT. The data presented in Fig. 4c give grounds to believe that in the prenoon hours, on average, the width of the cusp is slightly larger for $B_y < 0$ than for $B_y > 0$. A possible reason could be a shift of the cusp when $B_y > 0$ in the afternoon direction.

4. LATITUDE PROFILE OF ION PRECIPITATION IN THE CUSP REGION

The results of analyzing the structure of ion precipitation in the near-noon sector, especially in the region of polar cusp precipitation, can, according to

(Pitout and Bogdanova, 2021), be largely determined by the magnitude and direction of magnetospheric convection, depending on the B_z - and B_y -components of the IMF. As well, the B_z -component of the IMF will determine the meridional component of plasma convection in the magnetosphere and ionosphere, and B_y is the zonal component of convection. However, such simple ideas do not take into account the entire complex pattern of electric fields at cusp latitudes. The structure of large-scale electric field vortices at ionospheric heights is created during closing of large-scale field-aligned currents in the ionosphere and is governed mainly by both the values of large-scale pressure gradients and ionospheric conductivity. The complex system of field-aligned currents in the polar cusps (often called region 0 currents or currents in the cusp) significantly distorts the pattern of currents inside the cusp. Therefore, it is rarely possible to observe a sufficiently clear pattern. However, Tsyganenko and Andreeva (2018) successfully simulated distortion of the magnetic field in the cusp by diamagnetic currents, taking into account penetration of the B_y -component of the IMF into the cusp region.

4.1. Latitudinal Profiles of Ion Pressure in the Cusp for B_z IMF < 0

Convection in the cusp begins to change 1–2 min after changes in the external influence conditions. Taking this into account, to study the structure of ion precipitation in the cusp depending on the IMF components, only events in which the corresponding IMF component was relatively stable were selected. The stability of the IMF components was determined by the following conditions: during the 20-min interval before recording of cusp precipitation commenced, the absolute value of the sought IMF component exceeded 1.0 nT and the component did not change sign in this time interval. Such fairly rigorous conditions significantly reduced the statistical set of events. Thus, for a negative polarity of the B_z -component, only 33 cases of recording of the cusp were selected. In all these events, the latitudinal profiles of the energy flux of ion precipitation were analyzed. Two Fi maxima were detected in 17 flybys of the F7 satellite, one in the equatorial and the other in the polar part of the cusp, and in 16 flybys, the Fi profile had one clearly pronounced maximum in the equatorial part of the cusp. We refer to cusps with two maxima in the latitudinal Fi profile as “two max cusps” in contrast to the term “double cusp,” which implies two independent sources of particles.

One example of two max cusps was presented above in Fig. 2a. Below, we consider not latitudinal Fi profiles by the ion pressure profiles (Pi) in the cusp, as shown in Fig. 2b. There are the following reasons for using Pi . First, since the ion energy across the entire width of the cusp changes insignificantly, the latitudinal Fi and Pi profiles are very similar. Second, the

average Pi level in the cusp is significantly higher in the cusp than in the neighboring precipitation regions *LLBL* and the mantle (Vorobjev et al., 2020); therefore the cusp is the most striking feature on the Pi profile. Third, when Pi is used, it becomes possible to compare the ion pressure in the cusp with the solar wind dynamic pressure and the pressure in the magnetosheath that arises when there is a pressure balance at the magnetopause.

In Fig. 2b, the boundaries of the cusp in this satellite flyby are shown by vertical dashed lines. The average parameters of the interplanetary medium for this event in the 20 min interval prior to recording of the cusp are as follows: $\langle B_z \rangle = -3.9$ nT, $\langle B_y \rangle = -2.6$ nT, $\langle P_{sw} \rangle = 3.0$ nPa. If we return even earlier to Fig. 1b, then we can see that in the region of the equatorial boundary of the cusp in the latitude range $\sim 71.8^\circ - 72.5^\circ$ CGL, the energy of precipitating ions decreases with increasing latitude. More precisely, it drops sharply upon transition from the region of the high-latitude ring current, in accordance with (Antonova et al., 2018), to the cusp region. The change in electron energy in Fig. 1b also corresponds to this interpretation. In the region of the higher-latitude, polar maximum, the Ei value remains constant. The decrease observed in the equatorial part of the cusp Ei with increasing latitude is typical for periods of southern orientation of the IMF and antisolar plasma convection in the near-noon sector.

Figure 5a shows the latitudinal profile of ion pressure obtained by averaging 12 “two max cusps” recording events. The profile was obtained by superimposing epochs relative to the average position of the polar and equatorial boundaries of the cusp. The registration of the cusp by the F7 satellite were carried out in the pre-noon sector $\langle MLT \rangle = 11.1$. On average, the width of the “two max cusps” was $\sim 1.0^\circ$ latitude with an average value of the vertical IMF component $\langle B_z \rangle = -3.0$ nT. The B_z - and B_y -components in the events under consideration were approximately equal, and the average value of the B_y -component of the IMF in absolute value $\langle |B_y| \rangle = 2.8$ nT. The solar wind dynamic pressure approximately corresponded to its average undisturbed level $\langle P_{sw} \rangle = 2.8$ nPa. In latitudinal profile Pi , the equatorial maximum ion pressure is ~ 1.4 nPa ($Pi_{max}^1 = 0.5 P_{sw}$), and the poleward maximum ~ 1.0 nPa ($Pi_{max}^2 = 0.4 P_{sw}$) with a minimum between them at a level of ~ 0.8 nPa.

In all “two max cusps” events, the average energy of precipitating ions in the equatorial part of the cusp decreases with increasing latitude. The decrease in Ei begins $0.2^\circ - 0.4^\circ$ below the equatorial boundary of the cusp in the *LLBL* region and is recorded approximately to the minimum in the latitudinal profile Pi . Further, with increasing latitude, in approximately half the events, the average energy of precipitating ions remains unchanged, while in others, it increases weakly with increasing latitude.

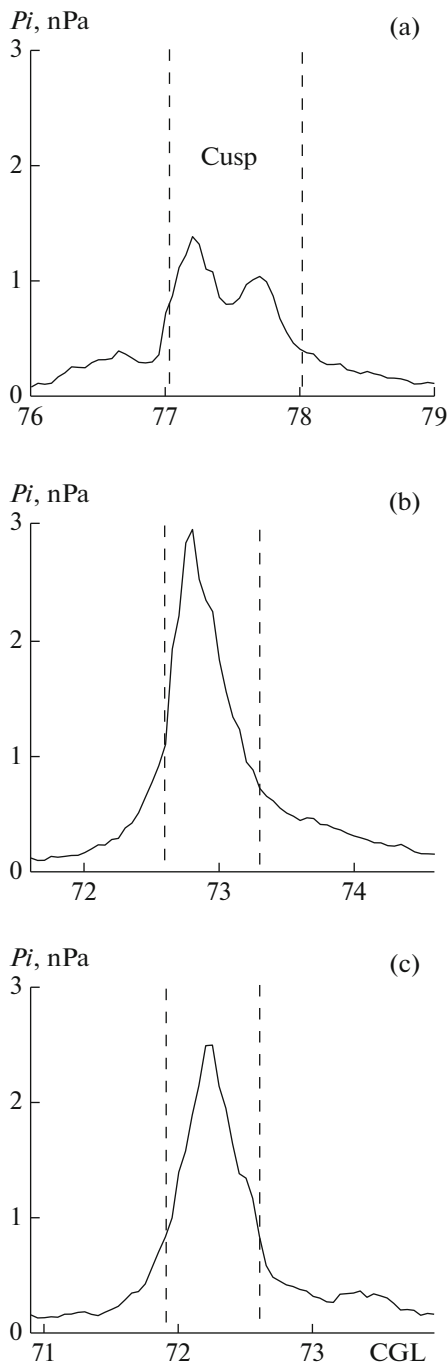


Fig. 5. Average latitude profiles of ion pressure (P_i) in cusp for negative values of B_z -component of IMF: (a) $\langle B_z \rangle = -3.0$ nT, $\langle |B_y| \rangle = 2.8$ nT; (b) $\langle B_z \rangle = -5.8$ nT, $\langle |B_y| \rangle = 3.1$ nT; (c) $\langle B_z \rangle = -7.1$ nT, $\langle |B_y| \rangle = 2.6$ nT. Vertical dashed lines are cusp boundaries.

Latitudinal profiles of ion pressure with one maximum can be divided into two types: with a P_i maximum shifted to the equatorial part of the cusp (12 flybys), and with a maximum approximately at the center of the cusp (4 flybys). The average profiles for these two types of distribution, obtained by superposed epoch analysis, are shown in Figs. 5b and 5c. In Fig. 5b, the P_i

maximum is located in the equatorial part of the cusp, the average width of the cusp $\langle \Delta\Phi \rangle = 0.7^\circ$, $\langle \text{MLT} \rangle = 11.7$, and the average values of the IMF components are as follows: $\langle B_z \rangle = -5.8$ nT, $\langle |B_y| \rangle = 3.1$ nT. The solar wind dynamic pressure during the recording period of profiles like $\langle P_{sw} \rangle = 4.0$ nPa, and the maximum ion pressure $\langle P_{i\text{max}} \rangle = 3.0$ nPa ($P_{i\text{max}} = 0.8 P_{sw}$).

Figure 5c shows the average latitudinal ion pressure profile with the P_i maximum at the center of the cusp. The average width of the cusp, as in Fig. 5b, is 0.7° ; the average MLT of recording is 12.2; and the values of the IMF components are as follows: $\langle B_z \rangle = -7.1$ nT, $\langle |B_y| \rangle = 2.6$ nT. The solar wind dynamic pressure $\langle P_{sw} \rangle = 3.8$ nPa; the maximum ion pressure $\langle P_{i\text{max}} \rangle = 2.6$ nPa ($P_{i\text{max}} = 0.7 P_{sw}$).

Comparison of Figs. 5a–5c shows that with increasing negative values of the B_z -component of the IMF, the cusp shifts to lower latitudes, the width of the cusp decreases, and the polar maximum vanishes (Figs. 5b, 5c).

4.2. Latitudinal Profile of Ion Pressure for B_z IMF > 0

For B_z IMF > 0 , to limit the influence of the B_y -component on the latitudinal profile of ion precipitation, some restrictions were imposed on the B_y : only flybys were considered in which, in a 20-min interval before recording of the cusp $|B_y| < 4$ nT and $|B_y| < 1.5 B_z$.

For relatively stable positive values of the IMF vertical component, profiles were observed in single events of P_i with various configurations: a wide profile with a flat top (three flybys) or a wide flat profile with a slight increase in P_i in the central part of the cusp (two flybys). However, the most characteristic of B_z IMF > 0 is profile P_i with the maximum ion pressure shifted to the polar part of the cusp (11 flybys). The average latitudinal profile of this type, obtained by superposed epoch analysis, is shown in Fig. 6a. The latitudinal width of the cusp for $B_z > 0$ is significantly greater than for $B_z < 0$ and average 1.4° of latitude; the average geomagnetic time of recording of the cusp is 11.6 MLT. The average parameters of the interplanetary medium are as follows: $\langle B_z \rangle = 2.2$ nT, $\langle |B_y| \rangle = 2.2$ nT, $\langle P_{sw} \rangle = 3.3$ nPa. The equatorial boundary of the cusp was at a latitude of $\sim 79^\circ$ CGL, which is $\sim 1.0^\circ$ CGL higher than in Fig. 5a at $\langle B_z \rangle = -3.0$ nT. The maximum ion pressure value $\langle P_{i\text{max}} \rangle = 1.3$ nPa ($P_{i\text{max}} = 0.4 P_{sw}$), which approximately corresponds to the maximum pressure in the cusp at close but negative values of the B_z -component of the IMF.

The behavior of the average ion precipitation energies with changes of latitude is ambiguous. Only in three of the considered events was the expected growth E_i observed for the periods $B_z > 0$ in the cusp or in its polar part with increasing latitude. The absence of dispersion or weak growth of E_i with increasing Φ' is more typical.

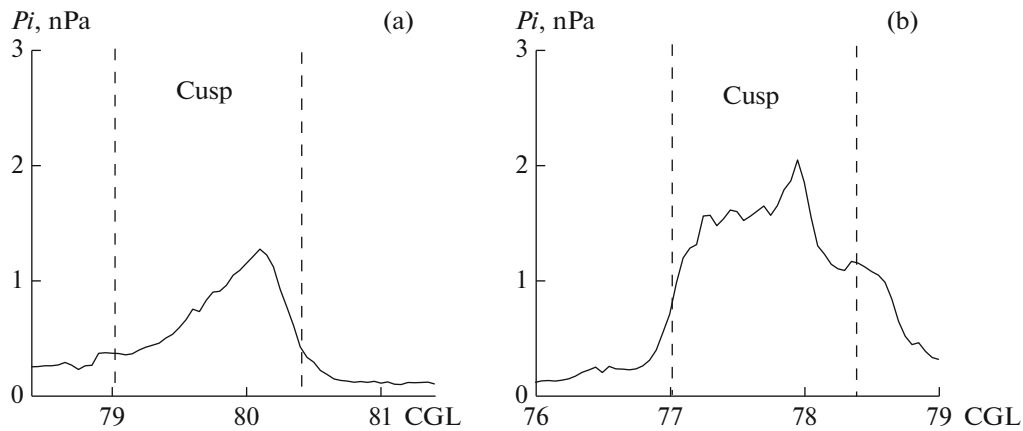


Fig. 6. Average latitude profiles of ion pressure in cusp: (a) for positive B_z -component of IMF, $\langle B_z \rangle = 2.2$ nT, $\langle |B_y| \rangle = 2.2$ nT; (b) for large negative B_y -component of IMF, $\langle B_y \rangle = -6.3$ nT, $\langle B_z \rangle = -1.7$ nT.

4.3. Latitudinal Profile of Ion Pressure for Large Values of the B_y -Component of the IMF

To study the influence the B_y -component of the IMF on the latitudinal profile of ion precipitation, events were selected that satisfied the following conditions: $|B_y| > 4.0$ nT and $|B_y| > 1.5|B_z|$. According to (Wing et al., 2001; Pitout et al., 2009), such conditions should be the most favorable for the formation of two sources of precipitating particles in the cusp and, accordingly, a double cusp. However, out of 31 cases of recording of cusp, when the B_y -component was the dominant one, in only 6 cases, the latitudinal P_i profile had two maxima in the cusp. In this study, we consider in more detail cusp recordings for $B_z < 0$ and large negative values of the B_y -component. Sixteen such events were recorded, of which for four crossings of the cusp, the latitudinal profile P_i had two maxima, one in the equatorial and the other in the polar part of the cusp. The most characteristic for periods with large negative B_y component is a wide cusp with a flat top in the latitudinal P_i profile and, in some cases, in the presence of a local maximum in any part of the cusp.

Figure 6b shows the average latitudinal ion pressure profile obtained by the superposed epoch analysis, for $B_z < 0$ and $B_y < 0$. The average width of the cusp is $\langle \Delta\Phi \rangle = 1.4^\circ$ CGL. Note the high level of ion precipitation at the polar boundary of the cusp and in the equatorial part of the mantle, amounting to more than 0.5 of the pressure level in the cusp. The average longitude of the cusp recording $\langle \text{MLT} \rangle = 11.1$. The average values of the parameters of the interplanetary medium were as follows: $\langle B_z \rangle \geq -1.7$ nT, $\langle B_y \rangle = -6.3$ nT, $\langle P_{sw} \rangle = 3.4$ nPa. The average ion pressure in the cusp does not exceed 2.0 nPa ($P_{i\text{max}} = 0.6P_{sw}$).

The average energy of precipitating ions in the cusp, as a rule, decreases with increasing latitude. Such E_i behavior indirectly indicates the antisolar direction of convection in the cusp region.

5. RADIAL PRESSURE PROFILE IN THE EQUATORIAL PLANE AT THE TRANSITION FROM THE MAGNETOSPHERE TO THE MAGNETOSHEATH

Unfortunately, there has been hardly any comparison of simultaneous observations of precipitation in the cusp with the results of high-apogee observations in the outer regions of the cusp, which would be extremely interesting when analyzing the processes of cusp formation and its dynamics. Therefore, for now, it is only possible to compare the averaged distributions at the intersection of the cusp with the averaged distributions in the magnetosheath obtained near the equatorial plane in the longitudinal sector of the cusp at close values of geomagnetic activity and the solar wind and IMF parameters. Vorobjev et al. (2022) demonstrated the efficiency of comparing DMSP data with publicly available THEMIS mission data (<http://themis.ssl.berkeley.edu/>, <http://cdaweb.gsfc.nasa.gov/>) for the nighttime sector. The present study uses the same THEMIS database, but for the midday sector.

Figure 7 shows the average variability of the pressure components in the equatorial plane, obtained by averaging flybys of THEMIS satellites in magnetically quiet conditions for Dst in the range from 0 to -10 nT and AL from 0 to -200 nT for a solar wind dynamic pressure of 1.5 to 3.5 nPa. Figure 7a shows the pressure components for $B_z < 0$, and Fig. 7b, for $B_z > 0$ in the angular sector $\pm 10^\circ$ from the noon meridian. The thick black line in the figure shows the integral pressure, with summation of the pressure of ions (solid thin line), electrons (dotted line), magnetic field (dashed line), and dynamic pressure (dashed line). Vertical segments contain the median values of the averaged values at a given geocentric distance.

For the southern and northern IMF, constant total pressure is observed, corresponding to the solar wind

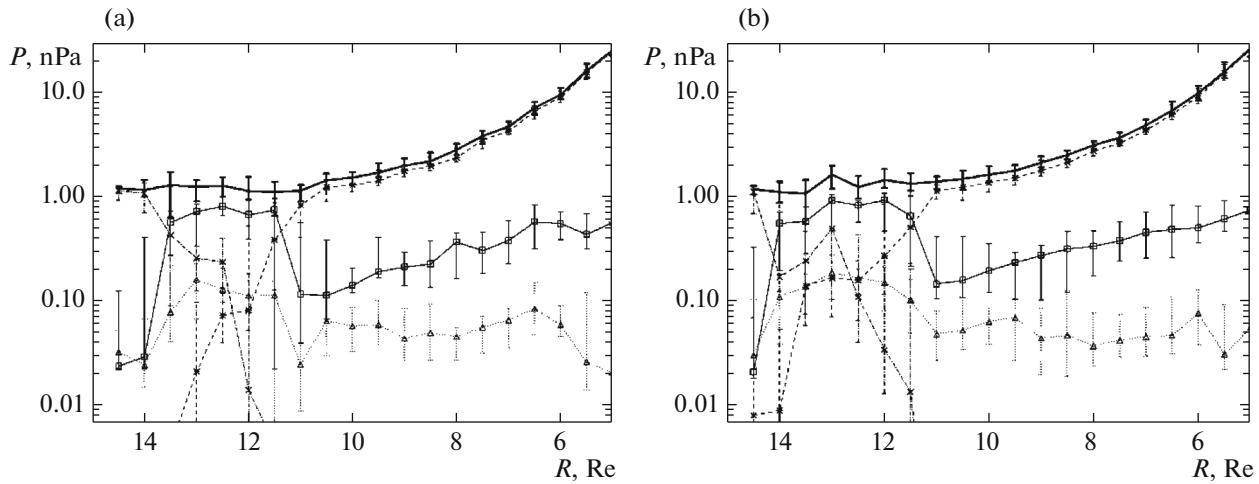


Fig. 7. Radial distribution of pressure components at transition from solar wind to magnetosphere for southern (a) and northern (b) orientation of IMF. Integral pressure is shown by solid thick curve; magnetic pressure, by dotted line; ion pressure, solid thin curve; electron pressure, by dotted curve; and dynamic pressure, by dotted line.

dynamic pressure from the solar wind in front of the bow-shock to the magnetosphere. After the magnetopause is crossed, the contribution of magnetic pressure becomes dominant. Within the magnetosheath, in accordance with Fig. 7, the main contribution to the integral pressure comes from thermalized ions. The averaged ion pressure profiles in the magnetosheath are nearly the same for southern and northern IMF orientations. The contribution of electrons is small throughout the studied interval, which well confirms the above assumption about the small contribution of electrons to pressure in the cusp. The difference in the variability of the radial pressure profiles for $B_z < 0$ and $B_z > 0$, as is known (see references in (Kirpichev et al., 2017)), occurs immediately before the magnetopause, where for $B_z < 0$, a relatively thin current sheet (thin magnetopause) appears with an abrupt transition from the magnetosheath to the magnetosphere; for $B_z > 0$, a fairly gradual transition from the magnetosheath to the magnetosphere is characteristic and a fairly extended region with a thickness of thousands of km (“thick” magnetopause) appears. In this case, a region can be identified in which a gradual increase in magnetic pressure compensates the drop in plasma pressure (*plasma depletion layer*), which may be directly related to the processes of magnetosheath plasma flux into the cusp region, the size and position of which is controlled by the IMF penetrating into the magnetosphere under conditions of magnetostatic equilibrium. It was noted in (Panov et al., 2008) that, when comparing the pressure in the magnetosheath and cusp, it is necessary to make a correction by multiplying the dynamic pressure in the magnetosheath by $\cos^2(\phi)\cos^2(\theta)$, where ϕ and θ are the geomagnetic latitude and longitude of the observation area. This correction for a cusp at a latitude of 72° near noon is ~ 0.01 . In accordance with Fig. 7, the main contribution to the pressure balance in the cusp

region comes from the thermal pressure of ions, which on average is ~ 0.8 of the solar wind dynamic pressure. This relationship between the maximum pressure in the cusp and solar wind dynamic pressure agrees well with the values in Fig. 5 for $B_z < 0$, when the cusp shifts to low latitudes. A poleward shift of the cusp leads to lower pressures in the cusp for $B_z > 0$. The magnitude of the relationship between the maximum pressure in the cusp and solar wind dynamic pressure for the northern orientation of the IMF requires additional analysis. Thus, the characteristics of the plasma in the cusp basically correspond to the characteristics of the plasma in the magnetosheath. Acceleration processes during particle interaction with turbulence in the cusp apparently do not lead to a significant change in pressure. Thus, pressure measurements in the cusp region by a low-altitude satellite contain information about the pressure in the cusp near the magnetopause, at least for $B_z < 0$, which is of interest when comparing predictions of magnetosphere formation models with experimental observational data.

The pressure distribution with a maximum in the cusp (Figs. 5b and 5c) well illustrates the formation of a diamagnetic cavity in the cusp region, where the maximum pressure corresponds to the region of minimum magnetic pressure at high altitudes. Such a maximum can only be tracked by a low-flying satellite, since high-apogee satellites move quite slowly and during the time of crossing the cusp region, the pressure distribution can change significantly. Therefore, information about the position of the pressure maximum can be used to improve models of the magnetic field in the cusp, constructed with allowance for currents in the cusp region, such as the model in (Tsyganenko and Andreeva, 2018), and to compare predictions of magnetic field models with specific fly-bys through the cusp at low heights.

Of particular interest are the cases with two pressure maxima shown in Fig. 5a, which cannot be easily explained by the developed models. In addition to the approach developed in (Wing et al., 2001), other explanations cannot be excluded. For example, penetrations of plasma jets through the magnetopause have been recorded (see references in (Pitout and Bogdanova, 2021)), the dynamic pressure in which is several times higher than the solar wind dynamic pressure. The penetration of such jets into the cusp can significantly change the equilibrium pattern of the ion pressure distribution. Recall also that the cusp is a funnel, the filling of which changes with changes in solar wind pressure, and its shape and size changes with changes in the IMF. The hydrodynamic structure of a funnel being filled is known to contain a minimum pressure at the center and a maximum at the edges. However, testing of such hypotheses, as well as models (Wing et al., 2001), requires thorough analysis of all available observational data at different heights, as well as and new measurements.

6. MAIN RESULTS

The review showed that analysis of crossings of low-flying satellites of polar cusp precipitation can provide new information on the properties and dynamics of cusps. In this study, data from the DMSP F7 satellite are used to study the specific features of the latitudinal distribution of the characteristics of precipitating ions in the region of the dayside polar cusp, as well as the ion pressure. The selection of F7 satellite flybys in the near-noon sector, during which the polar cusp was recorded, was done with data from an automated processing system (APS), developed on the basis of an artificial neural network (Newell et al., 1991). For most of the flybys selected in this manner, we analyzed the initial data from the F7 satellite, including determination of the latitude of its equatorial and polar boundaries. A significant difference in the average width of the cusp was discovered, amounting to $\sim 0.3^\circ$ of latitude, due to the difference in identification of its boundaries by the APS and direct analysis of satellite observations. The cusp width ($\Delta\Phi'$) was determined by the difference of latitude of its polar and equatorial boundaries. The average longitude of the satellite crossing the dayside polar cusp for the entire dataset is 11.3 MLT. Thus, all the results obtained are attributed to the prenoon MLT sector.

As a test, data from direct analysis of satellite observations were used to study the well-known dependence of the latitudinal position of the equatorial boundary of the cusp on the B_z -component of the IMF. The regression equations obtained individually for $B_z < 0$ and $B_z > 0$ best fit the data from (Wing et al., 2001), albeit with higher correlation coefficients.

The dependence of the latitudinal dimensions of the cusp on the B_z - and B_y -components of the IMF was studied. Linear regression equations with small

correlation coefficients $r = 0.47$ and $r = 0.25$ were obtained for the B_z - and B_y -components of the IMF, respectively. The range of $\Delta\Phi'$ values on the plots is significant, which may be governed by the effect of other parameters of external influence on the cusp width. However, the data obtained reliably indicate two significant factors. First, on average, the cusp is much wider for $B_z > 0$ than for $B_z < 0$. Second, the data obtained give grounds to believe that in the prenoon hours, on average, the cusp width is slightly larger for $B_y < 0$ than for $B_y > 0$.

The main goal of the article was to study the specific features of the latitudinal distribution of the characteristics of precipitating ions in the cusp region and their relationship with the B_z - and B_y - components of the IMF. The level of the ion pressure (P_i) as the main parameter characterising the latitudinal structure of ion precipitation in the cusp, which makes it possible to compare the ion pressure in the cusp with the solar wind dynamic pressure and pressure in the magnetosheath. Comparison of the obtained pressure distributions in the cusp with the averaged pressure distribution in the magnetosheath showed good agreement, which confirms the possibility of considering cusps in most cases as a diamagnetic cavity reaching ionospheric heights, the pressure in which is balanced by the (mainly ion) pressure in the magnetosheath.

Analysis of the entire dataset indicates that the nature of ion precipitation in the cusp is very variable. The latitudinal structure of precipitation in the cusp depends not only on the parameters of external influence and combinations thereof, but also on the time elapsed after a change in any of these parameters. Thus, the results obtained in this study should be considered as specific features of precipitation characteristic of a particular IMF component with its relative stability.

The main results can be formulated as follows.

(1) For negative values of the B_z -component of the IMF, a characteristic feature of the cusp is the latitudinal P_i profile with two maxima, one of which is located in the equatorial and the other in the polar part of the cusp, or a latitudinal profile with one clearly defined maximum in its equatorial part.

(2) On average, the width of the cusp with two maxima is $\sim 1.0^\circ$ of latitude for small and approximately equal values of the IMF components $\langle B_z \rangle = -3.0$ nT and $\langle |B_y| \rangle = 2.8$ nT. In the latitudinal P_i profile, the equatorial maximum ion pressure is $P_{i\max}^1 = 0.5 P_{sw}$, and in the polar, $P_{i\max}^2 = 0.4 P_{sw}$.

(3) For large negative values of the B_z -component ($|B_z| = 6-7$ nT), the polar maximum in the latitudinal P_i profile vanishes and only the equatorial maximum remains; the P_i level increases at a maximum $P_{i\max} = 0.8 P_{sw}$, and the width of the cusp decreases on average to $\langle \Delta\Phi' \rangle = 0.7^\circ$.

(4) For $B_z > 0$ the most characteristic profile is P_i with a maximum ion pressure in the polar part of the

cusps. The cusp is located at higher latitudes than for $B_z < 0$; its average latitudinal dimensions increase to an average of $\sim 1.4^\circ$ latitude. The maximum ion pressure $P_{\text{max}} = 0.4 P_{\text{sw}}$, which approximately corresponds to the maximum pressure in the cusp for close-in-magnitude, but negative B_z values.

(5) The most characteristic for periods with a large negative B_y -component ($\langle B_y \rangle = -6.3$ nT, $\langle B_z \rangle = -1.7$ nT) is a wide cusp with a flat top in the latitudinal P_i profile. The average cusp width is $\langle \Delta \Phi \rangle = 1.4^\circ$ CGL, and the ion pressure at maximum $P_{\text{max}} = 0.6 P_{\text{sw}}$.

(6) The ion pressure in the cusp is determined by the ion pressure in the magnetosheath in front of the cusp. The maximum ion pressure during observations at low heights may indicate the value of the plasma pressure in the magnetosheath in front of the cusp region.

7. CONCLUSION

Data from the low-altitude DMSP F7 satellite were used to analyze the latitudinal characteristics of ion precipitation in the dayside polar cusp and study the latitudinal profile of ion pressure in the cusp depending on the IMF parameters. It was shown that for small negative values of the B_z -component of the IMF, a characteristic feature of the cusp is the latitudinal profile of the ion pressure (P_i) with a width of $\sim 1^\circ$ latitude with two maxima, one of which is located in the equatorial and the other in the polar part of the cusp. For large negative B_z values, the polar maximum in the latitudinal P_i profile disappears; only the equatorial maximum remains, the P_i level at the maximum increases, and the width of the cusp decreases to $\sim 0.7^\circ$. For $B_z > 0$ the most characteristic profile is P_i with a maximum ion pressure in the polar part of the cusp. The cusp for $B_z > 0$ is located at higher latitudes than for $B_z < 0$, and its average latitudinal dimensions increase to $\sim 1.4^\circ$ of latitude. In the prenoon sector, MLT most typical for periods with a large negative B_y -component is a cusp with a width of $\sim 1.4^\circ$ of latitude with a flat top in the latitudinal P_i profile. Comparison of pressure distributions observed at low heights with data from high-apogee THEMIS satellites confirmed the possibility of describing the formation of the cusp as a diamagnetic cavity and using observations in the cusp to determine the ion pressure in the magnetosheath.

The results obtained in this study have made it possible to identify previously incompletely described features of the distribution of particle fluxes in cusps. Calculation of the ion pressure in the cusp at low heights and its comparison with the pressure in the magnetosheath made it possible to confirm the existence of a pressure balance in the region where the contribution of the magnetic field pressure is small or completely absent. The results of the study may be useful in creating magnetic field models taking into account diamagnetic currents in the cusp and in

describing cusp formation processes. The results may also be useful in implementing the SMILE space program. Cases of observations of pressure in the cusp at low heights require additional careful analysis.

ACKNOWLEDGMENTS

DMSP satellite data are taken from (<http://sd-www.jhuapl.edu>); parameters of the IMF, solar wind plasma, and magnetic activity indices are taken from (<http://wdc.kugi.kyoto-u.ac.jp/> and <http://cdaweb.gsfc.nasa.gov/>); THEMIS mission satellite data are taken from (<http://themis.ssl.berkeley.edu/>, <http://cdaweb.gsfc.nasa.gov/>).

FUNDING

Research carried out by V.G. Vorobyov was supported by the Russian Science Foundation, project no. 22-12-20017.

CONFLICT OF INTEREST

The authors of this work declare that they have no conflicts of interest.

REFERENCES

- Antonova, E.E. and Stepanova, M.V., The impact of turbulence on physics of the geomagnetic tail, *Front. Astron. Space Sci.*, 2021, vol. 8, p. 622570. <https://doi.org/10.3389/fspas.2021.622570>
- Antonova, E.E., Vorobjev, V.G., Kirpichev, I.P., and Yagodkina, O.I., Comparison of the plasma pressure distributions over the equatorial plane and at low altitudes under magnetically quiet conditions, *Geomagn. Aeron. (Engl. Transl.)*, 2014, vol. 54, no. 3, pp. 278–281. <https://doi.org/10.1134/S0016793214030025>
- Antonova, E.E., Vorobjev, V.G., Kirpichev, I.P., Yagodkina, O.I., and Stepanova, M.V., Problems with mapping the auroral oval and magnetospheric substorms, *Earth Planets Space*, 2015, vol. 67, no. 1, p. 166. <https://doi.org/10.1186/s40623-015-0336-6>
- Antonova, E.E., Stepanova, M., Kirpichev, I.P., Ovchinnikov, I.L., Vorobjev, V.G., Yagodkina, O.I., Riazan-seva, M.O., Vovchenko, V.V., Pulnits, M.S., Znatkova, S.S., and Sotnikov, N.V., Structure of magnetospheric current systems and mapping of high latitude magnetospheric regions to the ionosphere, *J. Atmos. Solar-Terr. Phys.*, 2018, vol. 177, pp. 103–114. <https://doi.org/10.1016/j.jastp.2017.10.013>
- Antonova, E.E., Stepanova, M.V., and Kirpichev, I.P., Main features of magnetospheric dynamics in the conditions of pressure balance, *J. Atmos. Sol.-Terr. Phys.*, 2023, vol. 242, p. 105994. <https://doi.org/10.1016/j.jastp.2022.105994>
- Baker, K.B. and Wing, S., A new magnetic coordinate system for conjugate studies at high latitudes, *J. Geophys. Res.*, 1989, vol. 94, no. A7, pp. 9139–9144. <https://doi.org/10.1029/JA094iA07p09139>
- Bogdanova, Y.V., Owen, C.J., Siscoe, G., Fazakerley, A.N., Dandouras, I., Marghitu, O., et al., Cluster observations of the magnetospheric low-latitude boundary layer

- er and cusp during extreme solar wind and interplanetary magnetic field conditions: I. 10 November 2004 ICME, *Sol. Phys.*, 2007, vol. 244, pp. 201–232. <https://doi.org/10.1007/s11207-007-0417-1>
- Escoubet, C.P., Berchem, J., Bosqued, J.M., Trattner, K.J., Taylor, M., Pitout, F., Vallat, C., Laakso, H., Masson, A., Dunlop, M., Reme, H., Dandouras, I., and Fazakerley, A., Two sources of magnetosheath ions observed by Cluster in the mid-altitude polar cusp, *Adv. Space Res.*, 2008, vol. 41, no. 10, pp. 1528–1536. <https://doi.org/10.1016/j.asr.2007.04.031>
- Esmaeili, A. and Kalaea, M.J., Double-cusp simulation during northward IMF using 3D PIC global code, *Astrophys. Space Sci.*, 2017, vol. 362, pp. 124–129. <https://doi.org/10.1007/s10509-017-3098-8>
- Fuselier, S.A., Trattner, K.J., and Petriner, S.M., Cusp observations of high- and low-latitude reconnection for northward interplanetary magnetic field, *J. Geophys. Res.*, 2000, vol. 105, no. A1, pp. 253–266. <https://doi.org/10.1029/1999JA900422>
- Kirpichev, I.P., Antonova, E.E., and Stepanova, M., Ion leakage at dayside magnetopause in case of high and low magnetic shears, *J. Geophys. Res.: Space Phys.*, 2017, vol. 122, no. 8, pp. 8078–8095. <https://doi.org/10.1002/2016JA023735>
- Newell, P.T. and Meng, C.-I., The cusp and the cleft/boundary layer: low-altitude identification and statistical local time variation, *J. Geophys. Res.*, 1988, vol. 93, no. A12, pp. 14549–14556. <https://doi.org/10.1029/JA093iA12p14549>
- Newell, P.T. and Meng, C.-I., Ionospheric projections of magnetospheric regions under low and high solar wind pressure conditions, *J. Geophys. Res.*, 1994, vol. 99, no. A1, pp. 273–286. <https://doi.org/10.1029/93JA02273>
- Newell, P.T., Meng, C.-I., Sibeck, D.G., and Lepping, R., Some low-altitude cusp dependence on interplanetary magnetic field, *J. Geophys. Res.*, 1989, vol. 94, pp. 8921–8927. <https://doi.org/10.1029/JA094iA07p08921>
- Newell, P.T., Wing, S., Meng, C.-I., and Sigillito, V., The auroral oval position, structure, and intensity of precipitation from 1984 onward: An automated on-line data base, *J. Geophys. Res.*, 1991, vol. 96, no. A4, pp. 5877–5882. <https://doi.org/10.1029/90JA02450>
- Newell, P.T., Sotirelis, T., Liou, K., Meng, C.-I., and Rich, F.J., Cusp latitude and the optimal solar wind coupling function, *J. Geophys. Res.*, 2006, vol. 111, p. A09207. <https://doi.org/10.1029/2006JA011731>
- Onsager, T.G., Kletzing, C.A., Austin, J.B., and MacKierman, H., Model of magnetosheath plasma in the magnetosphere: cusp and mantle particles at low-altitudes, *J. Geophys. Res.*, 1993, vol. 20, no. 6, pp. 479–482. <https://doi.org/10.1029/93GL00596>
- Panov, E.V., Buchner, J., Franz, M., Korth, A., Savin, S.P., Reme, H., and Fornacon, R.-H., High-latitude Earth's magnetopause outside the cusp: Cluster observations, *J. Geophys. Res.*, 2008, vol. 113, p. A01220. <https://doi.org/10.1029/2006JA012123>
- Pitout, F. and Bogdanova, Y.V., The polar cusp seen by Cluster, *J. Geophys. Res.*, 2021, vol. 126, no. 9. <https://doi.org/10.1029/2021JA029582>
- Pitout, F., Escoubet, C.P., Klecker, B., and Dandouras, I., Cluster survey of the mid-altitude cusp. Part 2: Large-scale morphology, *Ann. Geophys.*, 2009, vol. 27, pp. 1875–1886. <https://www.ann-geophys.net/27/1875/2009/>
- Pulinets M.S., Ryazantseva M.O., Antonova E.E., Kirpichev I.P. Dependence of magnetic field parameters at the subsolar point of the magnetosphere on the interplanetary magnetic field according to the data of the THEMIS experiment, *Geomagn. Aeron. (Engl. Transl.)*, 2012, vol. 52, no. 6, pp. 730–739.
- Rakhmanova, L., Riazantseva, M., and Zastenker, G., Plasma and magnetic field turbulence in the Earth's magnetosheath at ion scales, *Front. Astron. Space Sci.*, 2021, vol. 7, p. 616635. <https://doi.org/10.3389/fspas.2020.616635>
- Reiff, P.H., Hill, T.W., and Burch, J.L., Solar wind plasma injection at the dayside magnetospheric cusp, *J. Geophys. Res.*, 1977, vol. 82, no. 4, pp. 479–491. <https://doi.org/10.1029/JA082i004p00479>
- Ruohoniemi, J.M. and Greenwald, R.A., Statistical patterns of high-latitude convection obtained from Goose Bay HF radar observations, *J. Geophys. Res.*, 1996, vol. 101, no. A10, pp. 21743–21763. <https://doi.org/10.1029/96JA01584>
- Siscoe, G., Kaymaz, Z., and Bogdanova, Y.V., Magnetospheric cusps under extreme conditions: Cluster observations and MHD simulations compared, *Sol. Phys.*, 2007, vol. 244, pp. 189–199. <https://doi.org/10.1007/s11207-007-0359-7>
- Sonnerup, B.U., Paschmann, O.G., Papamastorakis, I., Sckopke, N., Haerendel, G., Bame, S.J., Asbridge, J.R., Gosling, J.T., and Russell, C.T., Evidence for magnetic field reconnection at the Earth's magnetopause, *J. Geophys. Res.*, 1981, vol. 86, pp. 10049–10067. <https://doi.org/10.1029/JA086iA12p10049>
- Stepanova, M., Antonova, E.E., and Bosqued, J.-M., Study of plasma pressure distribution in the inner magnetosphere using low-altitude satellites and its importance for the large-scale magnetospheric dynamics, *Adv. Space Res.*, 2006, vol. 38, no. 8, pp. 1631–1636. <https://doi.org/10.1016/j.asr.2006.05.013>
- Tsyganenko, N.A. and Andreeva, V.A., Empirical modeling of dayside magnetic structures associated with polar cusps, *J. Geophys. Res.*, 2018, vol. 123, no. A11, pp. 9078–9092. <https://doi.org/10.1029/2018JA025888>
- Vorobjev, V.G. and Yagodkina, O.I., Structure of dayside polar cusp precipitation during the northward interplanetary magnetic field, *Bull. Russ. Acad. Sci.: Phys.*, 2022, vol. 86, no. 12, pp. 1537–1541. <https://doi.org/10.3103/S1062873822120280>
- Vorobjev, V.G., Yagodkina, O.I., and Antonova, E.E., Ion pressure in different regions of the dayside auroral precipitation, *Geomagn. Aeron. (Engl. Transl.)*, 2020, vol. 60, no. 6, pp. 727–736. <https://doi.org/10.1134/S0016793220060146>
- Vorobjev, V.G., Yagodkina, O.I., Antonova, E.E., and Kirpichev, I.P., Influence of extreme levels of the solar wind dynamic pressure on the structure of nightside au-

roral precipitation, *Geomagn. Aeron. (Engl. Transl.)*, 2022, vol. 62, no. 6, pp. 704–710.
<https://doi.org/10.1134/S0016793222060160>

Wing, S. and Newell, P.T., Center plasma sheet ion properties as inferred from ionospheric observations, *J. Geophys. Res.*, 1998, vol. 103, no. A4, pp. 6785–6800.
<https://doi.org/10.1029/97JA02994>

Wing, S., Newell, P.T., and Onsager, T.G., Modeling the entry of magnetosheath electrons into the dayside ionosphere, *J. Geophys. Res.*, 1996, vol. 101, no. A6,

pp. 13 155–13 167.

<https://doi.org/10.1029/96JA00395>

Wing, S., Newell, P.T., and Rouhoniemi, J.M., Double cusp: Model prediction and observational verification, *J. Geophys. Res.*, 2001, vol. 106, no. A11, pp. 25 571–25 593.

<https://doi.org/10.1029/2000JA000402>

Publisher's Note. Pleiades Publishing remains neutral with regard to jurisdictional claims in published maps and institutional affiliations.